Photocatalysis

Deutsche Ausgabe: DOI: 10.1002/ange.201601494
Internationale Ausgabe: DOI: 10.1002/anie.201601494

# A Conductive Hybridization Matrix of $RuO_2$ Two-Dimensional Nanosheets: A Hybrid-Type Photocatalyst

*Jang Mee Lee[+], Eun Kyung Mok[+], Seul Lee, Nam-Suk Lee, Lamjed Debbichi, Hyungjun Kim,* and Seong-Ju Hwang**

***Abstract:*** *A universal methodology to efficiently improve the photocatalyst performance of semiconductors was developed by employing exfoliated $RuO_2$ two-dimensional nanosheets as a conducting hybridization matrix. The hybridization with a $RuO_2$ nanosheet is easily achieved by crystal growth or electrostatically derived anchoring of semiconductor nanocrystals on the $RuO_2$ nanosheet. An enhanced chemical interaction of inorganic semiconductor with hydrophilic $RuO_2$ nanosheet is fairly effective in optimizing their photocatalytic activity and photostability by the enhancement of charge separation and charge mobility. The $RuO_2$-containing nanohybrids show much better photocatalyst functionalities than do the graphene-containing ones. The present study clearly demonstrates that hydrophilic $RuO_2$ nanosheets are superior hybridization matrices, over the widely used hydrophobic graphene nanosheets, for exploring new efficient hybrid-type photocatalysts.*

As an emerging member of low-dimensional nanostructures, exfoliated two-dimensional (2D) nanosheets (NSs) of layered metal oxide, are an area of intense research interest because of its extremely high morphological anisotropy and valuable functionalities.[1,2] Among many metal oxide NSs, layered $RuO_2$ NSs show the highest electrical conductivity and sufficient chemical stability, which renders this material a useful building block for hybridization with a diversity of chemical species.[3,4] Since the exfoliated NS, which is very thin, can create a strong electronic coupling with hybridized species,[5] the hybridization with a metallic $RuO_2$ NS is expected to be effective in improving the photocatalytic activity of semiconducting inorganic solids through the enhancement of charge transfer (CT) and charge mobility. In fact, highly conductive graphene NSs have been widely employed as an efficient hybridization matrix for enhancing the photocatalyst performance of diverse semiconductors, thus leading to a great deal of research activity on this topic.[6] However, a strong self-stacking tendency of graphene NSs prevents homogeneous hybridization with photocatalyst crystals.[7] Additionally the hydrophobic nature of graphene is not favorable for achieving strong chemical interactions with polar photocatalyst materials. The absence of such drawbacks for graphene renders the exfoliated $RuO_2$ NSs a better hybridization matrix than graphene for a diversity of semiconducting materials. However, at the stage of this submission, we were unaware of another report[8] about the application of metallic $RuO_2$ NSs as a conducting hybridization matrix for exploring efficient hybrid photocatalysts.

In this work, exfoliated $RuO_2$ NSs are used as a conducting hybridization matrix for semiconductor nanocrystals of $Ag_3PO_4$ and CdS. The resulting $RuO_2$-based nanohybrids are tested as photocatalysts for the visible-light-induced generation of $O_2$ and $H_2$, and the photodegradation of organic molecules. Additionally the photocatalyst performance of the reduced graphene oxide (rG-O) based nanohybrids is also examined to estimate the relative efficiency of $RuO_2$ incorporation relative to the graphene addition. The dissimilar chemical interactions between $RuO_2$/rG-O and semiconductors are investigated with density functional theory (DFT) calculations and contact angle measurements.

The synthesis of monolayered $RuO_2$ NSs by the soft-chemical exfoliation process was evidenced by high-resolution transmission electron microscopy (HR-TEM), energy dispersive spectrometry (EDS), and atomic force microscopy (AFM) measurements (see Figure S1 in the Supporting Information). The $RuO_2$-$Ag_3PO_4$ nanohybrids were synthesized by the crystal growth of $Ag_3PO_4$ in the colloidal suspension of the exfoliated $RuO_2$ NSs (Figure 1 A). The details of the synthetic conditions are provided in the Supporting Information. The obtained nanohybrids with the $RuO_2$/$Ag_3PO_4$ ratios of 0.025, 0.05, 0.075, and 0.1 wt% are denoted as RA025, RA05, RA075, and RA1, respectively. As plotted in Figure 1 B, all the present RA nanohybrids exhibit typical X-ray diffraction (XRD) peaks of cubic silver orthophosphate phase (JCPDS no. 06-050), thus indicating the formation of $Ag_3PO_4$ crystals. No $RuO_2$-related Bragg reflections are observed, and strongly suggests a good dispersion of $RuO_2$ NSs. As demonstrated in the field emission-scanning electron microscopy (FE-SEM) images in Figure 1 C, all the present RA nanohybrids show spherical $Ag_3PO_4$ particles anchored on the $RuO_2$ NS. The intimate coupling between $RuO_2$ and $Ag_3PO_4$ is confirmed by HR-TEM analysis which shows the lattice fringes of $Ag_3PO_4$

[*] J. M. Lee,[+] E. K. Mok,[+] S. Lee, Prof. S.-J. Hwang
Department of Chemistry and Nanoscience
Ewha Womans University, Seoul 03760 (Korea)
E-mail: hwangsju@ewha.ac.kr
Dr. N.-S. Lee
National Institute for Nanomaterials Technology (NINT)
Pohang University of Science and Technology (POSTECH)
Pohang 37673 (Korea)
Dr. L. Debbichi, Prof. H. Kim
Graduate School of EEWS
Korea Advanced Institute of Science and Technology (KAIST)
Daejeon 34141 (Korea)
E-mail: linus16@kaist.ac.kr
[+] These authors contributed equally to this work.

Supporting information for this article can be found under: http://dx.doi.org/10.1002/anie.201601494.

  

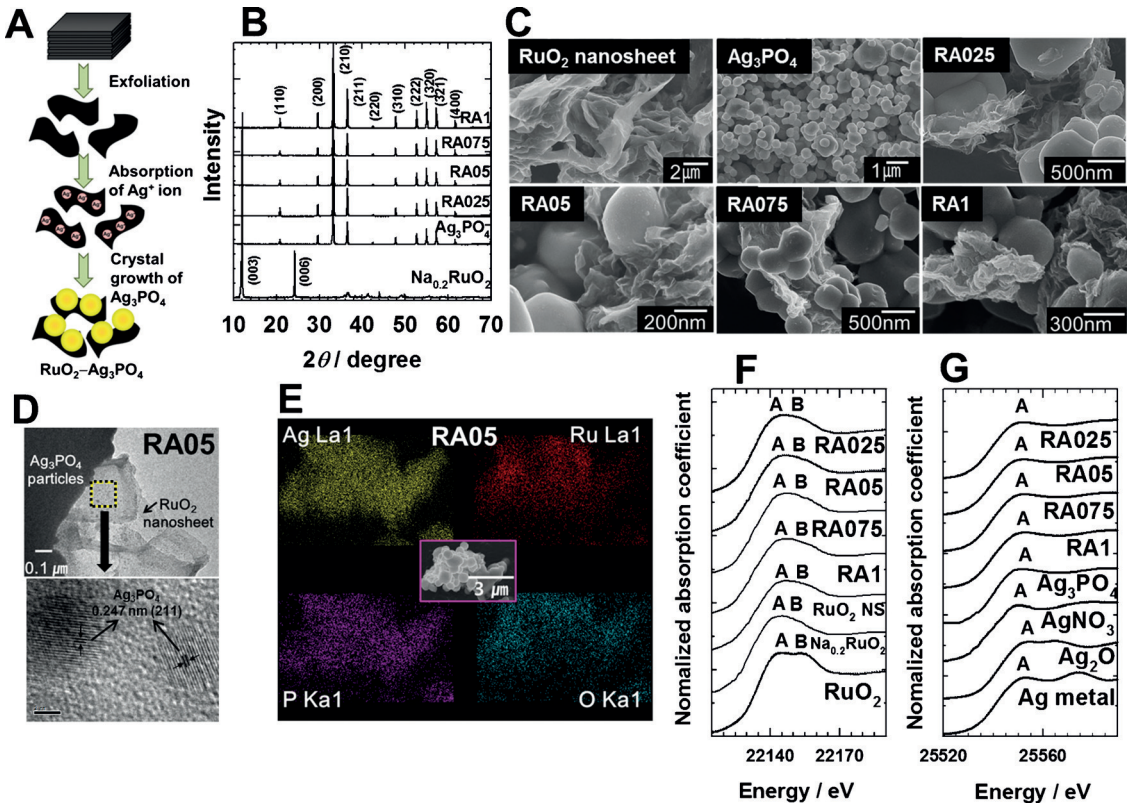


***Figure 1.*** A) Exfoliation and crystal growth route to the RA nanohybrid. Powder XRD patterns (B), FE-SEM images (C), HR-TEM images (D), EDS-elemental maps (E), and Ru K-edge (F) and Ag K-edge (G) XANES spectra of the RA nanohybrids and references.

nanoparticles immobilized on the $RuO_2$ NS (Figure 1D). EDS elemental mapping analysis provides clear evidence for the nanoscale mixing between these two components (Figure 1E). $N_2$ adsorption-desorption isotherm analysis demonstrates only a weak $N_2$ adsorption for all the RA nanohybrids, thus suggesting negligible contribution of surface expansion to the evolution of photocatalytic activity upon $RuO_2$ addition (see Figure S2). The maintenance of a layered $RuO_2$ structure upon hybridization with $Ag_3PO_4$ is evidenced by the Ru K-edge X-ray absorption near-edge structure (XANES) spectroscopy showing nearly identical features for the present RA nanohybrids and layered $RuO_2$ (Figure 1F). Similarly, all the RA nanohybrids commonly exhibit Ag K-edge XANES features which are nearly identical to that of $Ag_3PO_4$, thus reflecting the negligible effect of $RuO_2$ incorporation on the chemical bonding nature of $Ag_3PO_4$ (Figure 1G). The diffuse reflectance UV/Vis spectra in Figure 2A demonstrate that the increase of $RuO_2$ content in the RA nanohybrids enhances the absorption of visible light, thus confirming the successful incorporation of metallic $RuO_2$ NSs. As plotted in Figure 2B, the hybridization with $RuO_2$ NSs depresses the photoluminescence (PL) signal of $Ag_3PO_4$, thus underscoring the notable depression of the electron–hole recombination caused by CT from $Ag_3PO_4$ to $RuO_2$ (Figure 2C).

As can be seen clearly from Figure 2D, all the RA nanohybrids display photocatalytic activity, for visible-light-induced $O_2$ evolution ($\lambda > 400$ nm), which is higher than that of pure $Ag_3PO_4$, and underscores the beneficial effect of $RuO_2$ incorporation on the photocatalytic activity of $Ag_3PO_4$. Among the present materials, the RA05 nanohybrid with the intermediate $RuO_2/Ag_3PO_4$ ratio has the highest photocatalytic activity with a rate of 0.975 mmol $h^{-1}$ $g^{-1}$, which is much higher than that of unhybridized $Ag_3PO_4$ (0.597 mmol $h^{-1}$ $g^{-1}$). Similarly, all the RA nanohybrids can induce an efficient decomposition of methylene blue (MB) under visible-light ($\lambda > 420$ nm) irradiation. The rate of MB degradation is much faster for the **RA** nanohybrids than for the unhybridized $Ag_3PO_4$, thus confirming the beneficial role of $RuO_2$ NSs (Figure 2E). Taking into account the high electrical conductivity of the $RuO_2$ NS, this material is supposed to act as electron reservoir, conducting pathway, and cocatalyst in the present nanohybrid, much like the role of graphene in the graphene-based hybrid photocatalyst.[9] To investigate the relative efficiency of $RuO_2$ NS over the widely-used rG-O NS, the rG-O-$Ag_3PO_4$ nanohybrid with the rG-O/$Ag_3PO_4$ ratio of 0.05 wt% was also prepared by the same synthetic procedure (the obtained material is denoted as GA05). The hybridization between rG-O and $Ag_3PO_4$ is confirmed by powder XRD analysis and UV/Vis spectroscopy (see Figures S3 and S4). The hybridization of $Ag_3PO_4$ with rG-O leads to the depression of PL intensity, and is however less effective than that with $RuO_2$ NS (see Figure S5). This result provides strong evidence for a better role of $RuO_2$ NSs as a hybridization matrix than rG-O in enhancing the internal CT with $Ag_3PO_4$. As plotted in Figures 2D and E, the GA05 nanohybrid shows a lower photocatalytic activity for both $O_2$ evolution and MB degradation than does the RA05 nano-

  

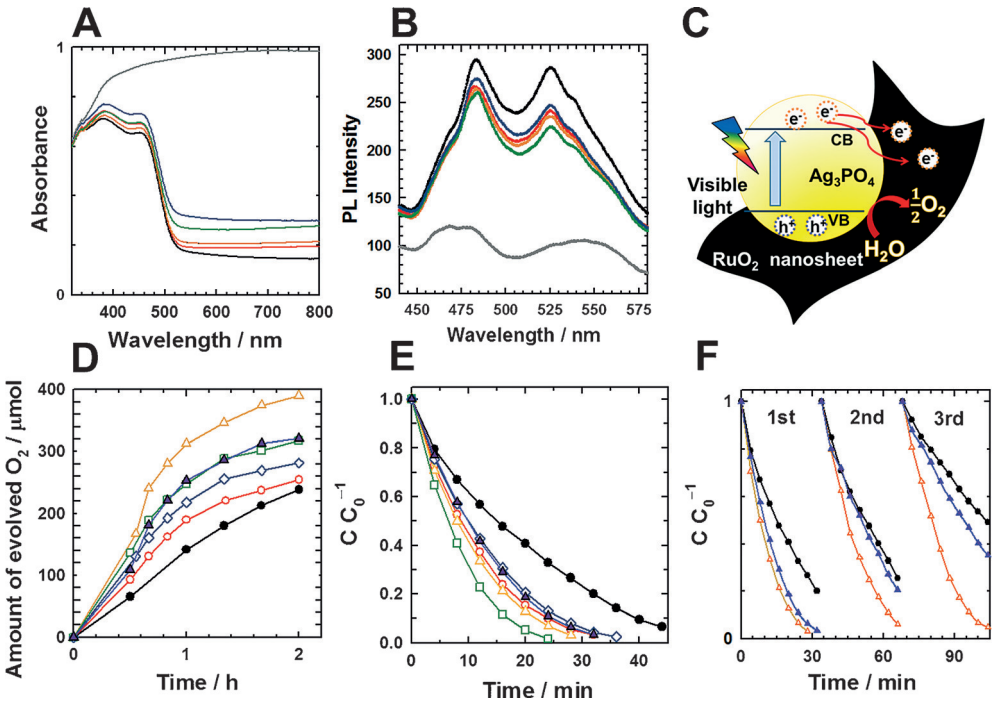


***Figure 2.*** Diffuse reflectance UV/Vis spectra (A), PL spectra (B), visible-light-induced $O_2$ evolution (D), visible-light-induced MB decomposition (E), and repeated tests (F) of photocatalytic activities of the pristine $Na_{0.2}RuO_2$ (gray), $Ag_3PO_4$ (black), RA025 (red), RA05 (orange), RA075 (green), RA1 (blue), and GA05 (purple). C) Model for internal electron transfer in the RA nanohybrids.

hybrid, thus highlighting the inferior role of rG-O over $RuO_2$ NSs in improving the photocatalytic activity of $Ag_3PO_4$. The hybridization effect on the photostabillity of $Ag_3PO_4$ was also tested with three successive photodegradations of MB (Figure 2F). In contrast to bulk $Ag_3PO_4$ which shows a marked degradation in photocatalytic activity, the RA05 nanohybrid displays only a negligible change. The improved photostability of $Ag_3PO_4$ upon the $RuO_2$ incorporation is attributable to an efficient migration of photoexcited electrons from $Ag_3PO_4$ to the $RuO_2$ NS, thus leading to the depression of the photoreduction of $Ag^+$ cation (Figure 2C). Such a beneficial effect of $RuO_2$ NS addition is more efficient than rG-O addition (Figure 2F). The present findings clearly demonstrate that the hybridization with $RuO_2$ NSs is fairly powerful for enhancing the photocatalytic activity and photostability of metal oxosalt.

To understand the better performance of the $RuO_2$ NSs than rG-O, their surface was examined with contact angle measurements (see Figure S6). While a wide contact angle of 84.1° is observable for the freestanding membrane of the rG-O NS, the $RuO_2$ membrane shows a much smaller contact angle of 26.6°, thus reflecting the higher surface hydrophilicity of $RuO_2$ than rG-O. The hydrophilic nature of the $RuO_2$ NS is responsible for more efficient chemical interactions and internal CT with polar $Ag_3PO_4$ particles, thus leading to the higher photocatalytic activity and photostability of the RA nanohybrid relative to that of GA. Ab initio DFT calculations further elucidate the atomic and electronic details of the hybrid interfaces between $RuO_2$/rG-O and $Ag_3PO_4$. First, we calculated the electronic band structure and density of states (DOS) of the isolated monolayer of $RuO_2$, and the data suggested that the major electronic conducting pathway within $RuO_2$ monolayer is by Ru atoms (Figure 3A). After the DFT optimization, we found the formation of Ag–O bonds at the $RuO_2$/$Ag_3PO_4$ interface, thus inferring the strong hybridization between $RuO_2$ and $Ag_3PO_4$ surfaces (Figure 3B). The distance between the layer and the surface is 2.2 Å (cf. Ag–O van der Waals (vdW) distance = 3.2 Å). This distance is in stark contrast to the graphene/$Ag_3PO_4$ interface, which shows a marginal geometrical change from their isolated structures (Figure 3C) with the atomically flat graphene sheet and a contact distance of 3.2 Å (cf. C–O vdW distance = 3.2 Å), thus indicating the covalent nature of $RuO_2$/$Ag_3PO_4$ interface and the vdW-type nature of the graphene/$Ag_3PO_4$ interface. The stronger interfacial hybridization of $RuO_2$/$Ag_3PO_4$ over graphene/$Ag_3PO_4$ is consequently reflected by the larger CT at the interface. As the charge density differences show in Figures 3D and E, the $RuO_2$/$Ag_3PO_4$ interface exhibits around tenfold more profound CT compared with that of graphene/$Ag_3PO_4$. The CT direction for $RuO_2$/$Ag_3PO_4$ is opposite for that of graphene/$Ag_3PO_4$, that is, CT from $Ag_3PO_4$ to $RuO_2$ versus CT from graphene to $Ag_3PO_4$. The former case yields a local electric field from $Ag_3PO_4$ to $RuO_2$ and helps the separation of excited electron from $Ag_3PO_4$ to the hybridization matrix while leaving a hole in the $Ag_3PO_4$. We also found that CT at the $RuO_2$/$Ag_3PO_4$ interface occurs for the entire $RuO_2$ sheet and for several atomic layers of the $Ag_3PO_4$ surface, while CT at the graphene/$Ag_3PO_4$ interface mostly occurs between graphene and only the top layer of $Ag_3PO_4$ surface. Our DFT results clearly indicate the existence of a much stronger donor–acceptor interaction in the $RuO_2$/$Ag_3PO_4$ interface, thus helping the excited electron-hole separation. A strong hybridization between the $RuO_2$ nanosheet and $Ag_3PO_4$ is confirmed by the observation of micro-Raman feature of the Ag–O interaction (see Figure S7).

The universal merit of $RuO_2$ hybridization in improving the photocatalytic activity of a semiconductor is further evidenced by the comparative investigation for the nanohybrids of $RuO_2$-CdS and rG-O-CdS with the $RuO_2$/CdS or rG-O/CdS ratio of 0.5 wt% (see Figures S8 and S9). As presented in Figure 4, the hybridization with $RuO_2$ NSs is much more effective in improving the visible light ($\lambda >$

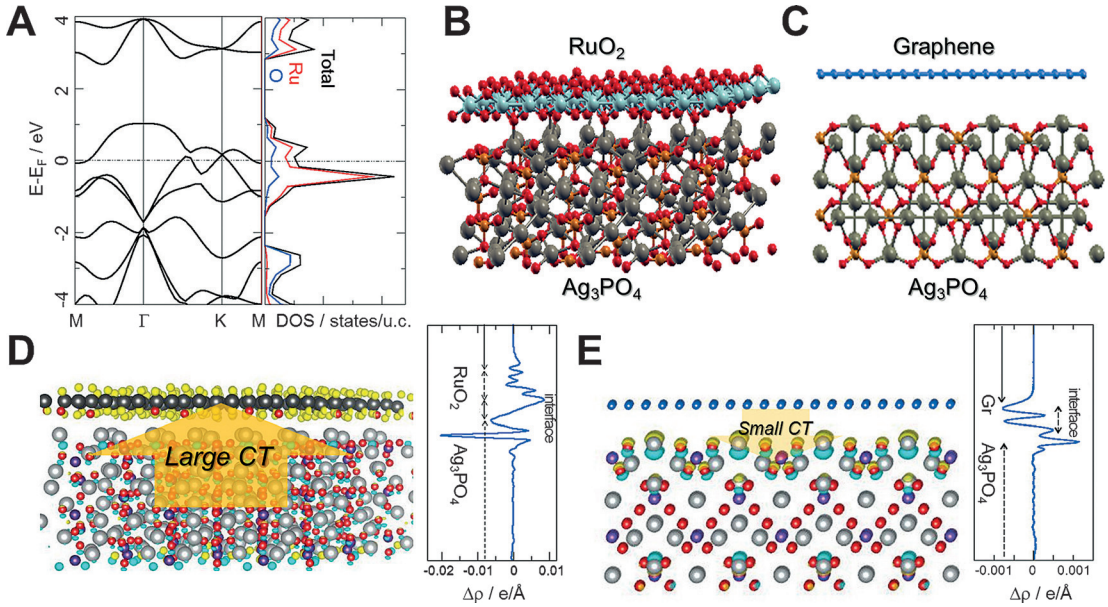


***Figure 3.*** A) Electronic band structure and density of states of the isolated $RuO_2$ sheet. Side-views of DFT optimized atomistic structures of $RuO_2$/$Ag_3PO_4$(111) interface (covalent type; B) and C) graphene/$Ag_3PO_4$ (100) interface (vdW type; C). Ag gray, O red, P orange, C blue, and Ru aquamarine. Charge density differences ($\rho$) of the $RuO_2$/$Ag_3PO_4$ (D) and graphene/$Ag_3PO_4$ (E) hybrid interface. In the left panels, charge density differences are shown three-dimensionally; the yellow and cyan regions represent charge accumulation and depletion, respectively. In the right panels, the planar-averaged charge density differences are plotted along the surface normal direction (chosen as the *z*-direction).

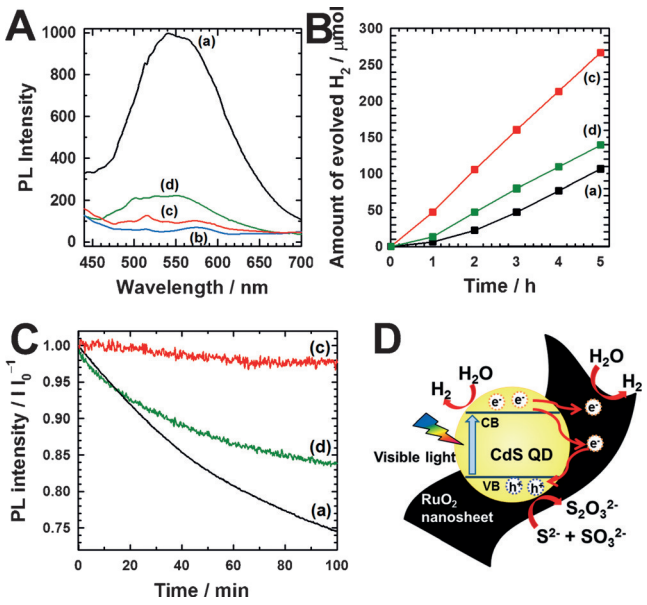


***Figure 4.*** PL spectra (A), visible-light-induced $H_2$ generation (B), and photostability test (C) of CdS QD (a), $Na_{0.2}RuO_2$ (b), $RuO_2$-CdS nanohybrid (c), and rG-O-CdS nanohybrid (d). D) Model for internal electron transfer in the $RuO_2$-CdS nanohybrid.

420 nm) photocatalytic activity of CdS quantum dots for $H_2$ production and photocurrent generation (see Figure S10), and its photostability, and is ascribable to the depression of the electron-hole recombination. The importance of the very thin exfoliated $RuO_2$ nanosheet in improving the photocatalyst activity of the semiconductor is evidenced by the efficient generation of $H_2$ by the $RuO_2$-CdS nanohybrid relative to that of the nanohybrid of CdS and unexfoliated $Na_{0.2}RuO_2$ material (see Figure S11). This result highlights a beneficial role of the $RuO_2$ NS in exploring highly efficient hybrid photocatalyst. In conclusion, we have developed a novel universal hybridization route to efficient photocatalyst materials by employing exfoliated $RuO_2$ 2D NSs as a conducting hybridization matrix. Despite the lower electrical conductivity of $RuO_2$ (833 $S\,cm^{-1}$) relative to graphene (6000 $S\,cm^{-1}$),[10,11] the hybridization with hydrophilic $RuO_2$ NSs is more effective in improving the photocatalytic activity and photostability of semiconductor nanocrystals compared with that with hydrophobic rG-O. This result is attributable to more efficient CT between $RuO_2$ and semiconductors, thus highlighting the importance of a chemical interaction between the hybridized components in optimizing the photocatalyst performance of nanohybrids. The present $RuO_2$-based nanohybrids show higher photocatalytic activity than do the well-known N- and Pt-doped $TiO_2$ materials, thus confirming the promising photocatalyst performance of the present nanohybrids (see Figure S12). Even though ruthenium is more expensive than carbon, this element is 20 times cheaper than platinum, which is widely used as a cocatalyst for photocatalyst systems.[12] Taking into account the fact that the hybridization with graphene has led to a great deal of research devoted to the graphene-based hybrid photocatalysts,[9] the present study should lead to new opportunities for the exploration of new $RuO_2$ NS-based hybrid photocatalysts.

## Acknowledgments

This work was supported by the Global Frontier R&D Program (2013-073298 and 2013M3A6B1078884) on Center

  

for Hybrid Interface Materials (HIM) from the National Research Foundation of Korea (NRF) on a grant funded by the Korea government (MSIP) (No. NRF-2014R1A2A1A10052809). The experiments at PAL were supported in part by MOST and POSTECH.

**Keywords:** conducting materials · graphene · nanostructures · photocatalysis · semiconductors

**How to cite:** *Angew. Chem. Int. Ed.* **2016**, *55*, 8546–8550
*Angew. Chem.* **2016**, *128*, 8688–8692

[1] J. Tao, T. Luttrell, M. Batzill, *Nat. Chem.* **2011**, *3*, 296–300.
[2] B. P. Bastakoti, Y. Li, M. Imura, N. Miyamoto, T. Nakato, T. Sasaki, Y. Yamauchi, *Angew. Chem. Int. Ed.* **2015**, *54*, 4222–4225; *Angew. Chem.* **2015**, *127*, 4296–4299.
[3] M. Osada, T. Sasaki, *Adv. Mater.* **2012**, *24*, 210–228.
[4] T. Sasaki, Y. Ebina, Y. Kitami, M. Watanabe, *J. Phys. Chem. B* **2001**, *105*, 6116–6121.
[5] C. N. R. Rao, H. S. S. R. Matte, U. Maitra, *Angew. Chem. Int. Ed.* **2013**, *52*, 13162–13185; *Angew. Chem.* **2013**, *125*, 13400–13424.
[6] Z. Zeng, T. Sun, J. Zhu, Z. Huang, Z. Yin, G. Lu, Z. Fan, Q. Yan, H. H. Hng, H. Zhang, *Angew. Chem. Int. Ed.* **2012**, *51*, 9052–9056; *Angew. Chem.* **2012**, *124*, 9186–9190.
[7] Q. J. Xiang, J. G. Yu, M. Jaroniec, *Nanoscale* **2011**, *3*, 3670–3678.
[8] K. Fukuda, T. Saida, J. Sato, M. Yonezawa, Y. Takasu, W. Sugimoto, *Inorg. Chem.* **2010**, *49*, 4391–4393.
[9] Q. Xiang, B. Cheng, J. Yu, *Angew. Chem. Int. Ed.* **2015**, *54*, 11350–11366; *Angew. Chem.* **2015**, *127*, 11508–11524.
[10] J. Sato, H. Sato, M. Kimura, K. Fukuda, W. Sugimoto, *Langmuir* **2010**, *26*, 18049–18054.
[11] X. Du, I. Skachko, A. Barker, E. Y. Andrei, *Nat. Nanotechnol.* **2008**, *3*, 491–495.
[12] InvestmentMine. (**2016**, Jan. 29). Retrieved from http://www.infomind.com/investment/metal-prices.

Received: February 11, 2016
Revised: April 19, 2016
Published online: May 31, 2016

  